Editors' Suggestion

Study of the high pressure phase evolution of Co_3O_4

Federico Cova,* Maria Valeria Blanco, Michael Hanfland, and Gaston Garbarino
European Synchrotron Radiation Facility, 71 Avenue des Martyrs, 38000 Grenoble, France

(Received 3 May 2019; revised manuscript received 2 August 2019; published 26 August 2019)

We present the study of the structural changes of cobalt oxide Co_3O_4 under high pressure. At room temperature and atmospheric pressure, Co_3O_4 crystallizes in a cubic Fd-$3m$ structure. We found that within the pressure range 0–60 GPa the system undergoes three phase transitions, which take place at 23, 45, and 52 GPa. In the first one, the original cubic structure distorts to an $Fddd$ orthorhombic lattice. At 45 GPa, a first order phase transition induces a distortion to a monoclinic phase with $C2/m$ space group and a volume per formula unit reduction of 4%. This phase has not been reported in the literature previously. Finally, at 52 GPa the orthorhombic phase disappears and a phase transition towards the formation of $P2_1/c$ crystal structure is evidenced. This last phase coexists with the $C2/m$ phase up to 55 GPa. From the diffractograms measured at 57 GPa it was possible to solve the structure of the $P2_1/c$ phase. Results showed the layered character of the structure and a change in the Co^{+2} coordination number from 4 to 6.

DOI: 10.1103/PhysRevB.100.054111

I. INTRODUCTION

Cobalates are AB_xO_n structures, where the A or B site is occupied by Co while the other metal site is occupied by a rare earth, transition, or post-transition metal. These compounds have shown several interesting properties [1,2], such as magnetic frustration in the A site, which causes $CoAl_{(1-x)}Co_xO_4$ to form a spin liquid in the entire x range [3]. In other cobalates, like $PrCoO_3$, the Jahn-Teller active Co^{+3} ions located in the B site are in an intermediate spin state, which induces octahedron distortion [4]. In particular, spinel Co_3O_4 is a p-type semiconductor that presents highly reactive exposed crystal planes [5]. Due to these particular properties, spinel Co_3O_4 has been utilized in different fields of technology, ranging from solid-state sensors and electrochemical devices to solar energy absorbers and hydrogen production [2,6–13]. More recently, it has been considered as a promising material for applications in emerging technologies like lithium batteries [14,15] and catalysis for low-temperature CO oxidation and the oxygen evolution reaction [7,16].

The study of the catalytic effect of the different planes of Co_3O_4 and its influence in various different reactions is a very rich field [5,16,17]. Since the configuration of the atoms on the surface is of key importance to determine the catalytic properties of Co_3O_4, the possibility of finding new phases that could present different atomic distributions in the exposed planes is very interesting. It is known that when a material is subjected to very high pressures interatomic distances are reduced, which results in the modification of the electronic configuration, leading to possible changes in the chemical and physical properties. In the case of spinels, it has been previously observed that the increase of pressure causes an alteration of the magnetic exchange interactions in the ferromagnetic to antiferromagnetic transition [18,19].

Previous studies on the properties of Co_3O_4 were mainly focused in the spinel structure. Only a few works reported the crystal structure evolution at high pressures, experimentally [20,21] or theoretically [22]. In a work presented by Hirai and Mao [20], it is stated that the system presents hysteresis, retaining the high pressure phase during decompression at a pressure more than 30 GPa lower than the observed for the transition during compression. The possibility of retaining a different phase at lower pressures is very interesting, since this phase and the different exposed planes that it presents on its surface could have very distinct properties than those observed in the common spinel structure. However, in order to take advantage of the potential opportunities that this new phase might bring, it is essential to adequately understand the behavior of the system at high pressures. Unfortunately, when considering the current scientific literature on Co_3O_4, this behavior remains unclear.

Different studies of the spinel Co_3O_4 system have reported contradictory results of its behavior under high pressure. Based on XANES results, Bai *et al.* [21] proposed that at 17.7 GPa, a charge transfer exists between the Co ions occupying the A and B sites in the system, leading to a transition from normal to a partially inverted spinel. According to their results, the system retains the same Fd-$3m$ cubic structure up to 42.1 GPa, with the mentioned electron transference as the only change. In *a posterior* work, Hirai and Mao [20] disputed this, reporting that the system presents a transition to a monoclinic structure above 30 GPa, which maintains up to 55 GPa. In the same work the authors also report a further transition to a different monoclinic phase during decompression. In their experiment, Hirai and Mao compressed Co_3O_4 from ambient to 54 GPa using neon as a pressure transmitting medium. While Ne can be considered as an adequate pressure transmitting medium at pressures up to 15 GPa [23], above this pressure its hydrostaticity starts to deviate from the ideal. This may lead to externally induced phase transitions in the system that would not occur under ideal conditions.

*federico.h.cova@ntnu.no

Theoretical calculations by Kaewmaraya *et al.* [22] predicted a transition from spinel Co_3O_4 to a layered monoclinic structure at 35 GPa but with different lattice parameter values than those reported by Hirai and Mao. The authors also concluded that the second monoclinic phase observed by Hirai and Mao upon decompression was not stable from an energetic point of view.

The main goal of this work is to present a detailed study of the structural changes of Co_3O_4 at high pressures. We performed synchrotron powder x-ray diffraction measurements of Co_3O_4 coupled with Raman spectrometry analysis in the pressure range 0–60 GPa. Special attention was given to the 20–55 GPa pressure range, at which the experimental data available is scarce and the reported results are contradictory.

II. EXPERIMENT

Co_3O_4 powder (particle size <10 μm, Sigma Aldrich) was loaded in a membrane driven diamond anvil cell (DAC). Based on previous reports on different pressure transmitting media [23,24], He was selected as PTM in order to ensure the best possible hydrostatic conditions up to the highest applied pressure.

The diamonds cullet size was 300 μm. A stainless steel gasket with a $\sim$160 μm diameter and 37–42 μm thickness hole was used. Ruby fluorescence was the method selected for pressure determination, using the scale proposed by Mao *et al.* [25]. High pressure synchrotron powder x-ray diffraction measurements were performed at the ID15B-High Pressure Diffraction Beamline of the ESRF, using a monochromated beam with an energy of 30 keV (wavelength 0.411 Å) and focused below 10×10 μm^2 using Be refractive lenses. The two-dimensional (2D) diffraction images were collected in a mar555 flat panel detector situated 400 mm behind the sample. The 2D images were integrated using Fit2D [26].

The XRD patterns were refined by the Rietveld method as implemented in the GSAS II package [27] and Fullprof suite [28]. The Le Bail method was utilized to determine the unknown crystal structures, and atomic positions were obtained using the charge flipping algorithm Superflip [29]. This procedure was performed using the Jana2006 software [30].

Complementary Raman spectroscopy measurements were performed using an in-house Raman setup available at ID15B. The setup was equipped with an Andor iDus 401 CCD detector and a Andor SR-500i-A-R spectrometer to acquire the measured spectra. Measurements were performed using a Cobolt Samba 150 green laser with wavelength of 532 nm focused at the sample position using a 20X Mitutoyo PLAN Apo infinity corrected long working distance objective.

Co_3O_4 was compressed up to 60 GPa using steps of approximately 0.3 GPa in the range ambient–3.5 GPa, and 1 GPa afterwards. In the regions in which phase transitions were observed, the step was reduced. Four independent experiments, three XRD and one Raman spectroscopy, were performed using different samples and cells, and in two of them it was also possible to obtain XRD patterns during decompression.

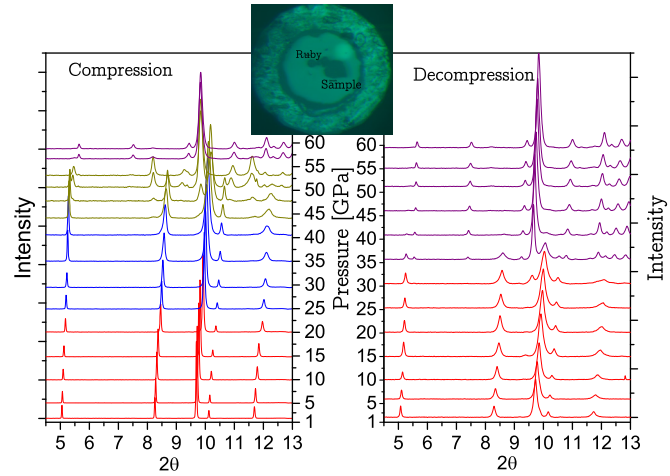

FIG. 1. XRD patterns showing the evolution of Co_3O_4 during compression (left) and decompression (right). Colors indicate the pressure ranges with different main phases. The inset displays a picture of one the loadings at 10 GPa, showing the relative position of the sample and the ruby.

III. RESULTS AND DISCUSSION

In the left panel of Fig. 1 a typical compression sequence obtained from one of the x-ray diffraction runs is presented. In this figure it is possible to observe within the 20–25 GPa region, a noticeable increment in the width of some of the reflections (see peaks at 8, 9.5, and 12 deg, the rest remain unchanged). Close to 45 GPa, the appearance of new reflections, coexisting with the low pressure ones, is evidenced. This is indicative of a first order phase transition. The peaks of the original phase disappear completely at pressures above 52 GPa, when other new reflections are observed, indicating a new phase transition. It is possible to assume that this new transition is also of first order, as demonstrated from the coexistence of two phases in the range of pressures between 52 and 55 GPa. Above 55 GPa, only the peaks corresponding to the new phase remain. This is an indication that this phase is the stable one at high pressures. The right panel of Fig. 1 shows the evolution of the diffractograms corresponding to the same sample during the decompression process that followed the one shown in the left part. It is evident from this plot that the system returns using a different path that the one followed during compression, with only one phase transition at around 35 GPa.

The experimental data measured at the initial pressure was fitted using the known Fd-3m structure with very good agreement with previous results ($a = 8.0912$ Å) [21,31,32]. The Rietveld refinement results obtained for the starting structure are presented in Fig. 2(a). This structure was used to refine sequentially the data up to 22 GPa. At higher pressures, the proposed structure did not fit properly the measured data, indicating that it is not an adequate model for the structure of the material.

In Fig. 3 the evolution with pressure of the full width at half maximum (FWHM) of the three first reflections, (111), (002), and (113), belonging to the cubic phase are plotted. A sudden increase of the broadening of (002) and (113) peaks occurs

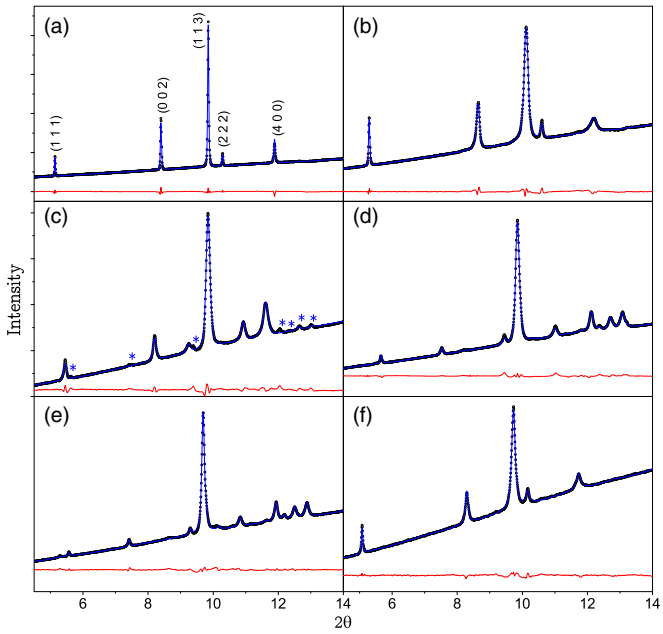

FIG. 2. Experimental data and the corresponding Rietveld refinement of the cubic phase at 2 GPa (a) during compression and ambient pressure during decompression (f), orthorhombic phase at 42 GPa (b) and $P2_1/c$ phase at 57 GPa (d) during compression and 37 GPa (e) during decompression, including the respective difference curves. (c) The experimental data of the $C2/m$ phase at 52 GPa and the corresponding LeBail fitting. The asterisks indicate reflections belonging to the $P2_1/c$ phase. In the cubic phase, the reflections are labeled to facilitate the identification of the peaks analyzed.

at $P > 22$ GPa, while (111) FWHM remains almost constant. This is in agreement with the deterioration of the goodness of fit observed when using the cubic phase for the refinement.

In order to better determine the critical pressure at which this structural change takes place, the low pressure dependence of the FWHM of (002) and (113) peaks was fitted with a linear function, and the pressure at which the experimental data starts to deviate from this line (25 GPa) was selected as the critical pressure.

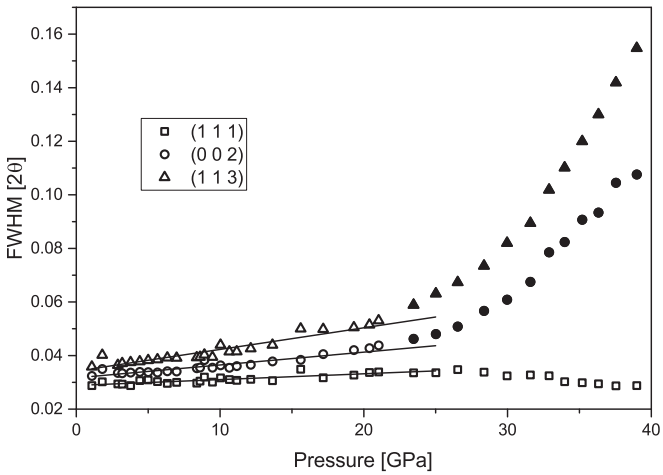

FIG. 3. FMHW of the (111), (002), and (113) reflections of the cubic phase of spinel Co_3O_4 as a function of pressure, obtained by fitting a single pseudo-Voigt peak. The lines are linear fit of the low pressure data (cubic phase represented by open symbols). The solid black symbols correspond to the orthorhombic phase.

TABLE I. Calculated parameters of the Vinet equation obtained from the fittings of the experimental data.

Phase	V_0	K_0	$K_0'(fix)$
Cubic	528(1)	224.3(9)	4
Orthorhombic	513(3)	321(8)	4

The abrupt raise observed in the peak broadening of some reflections is an indication that the material is suffering a distortion that leads to a lower symmetry crystal structure. Since the number of peaks and position are the same as in the spinel structure, an orthorhombic structure with lattice parameters very similar to the ones in the original structure was proposed. In an orthorhombic structure, a small variation in between the different lattice parameters would result in the splitting of some of the reflections. This would lead to a broadening of some of the peaks originally present in the cubic structure, which is consistent with the experimental results. On this basis, the refinements up to 45 GPa were performed using an orthorhombic phase with $Fddd$ space group. For this new fitting, the initial atomic positions were selected to match the positions of the same atoms in the cubic structure. Figure 2(b) shows the diffraction pattern corresponding to the orthorhombic phase at 42 GPa. It is possible to notice that (111) and (222) reflections, which do not split, present little broadening compared to their counterparts in the cubic phase. Considering this transition, the broad peaks observed at pressures higher than 25 GPa are the superposition of three different peaks of the orthorhombic structure. To illustrate this in the figure, the FWHM that correspond to more than one superimposed peak are represented with filled symbols.

The existence of this phase transition can be supported by comparing to theoretical results. The phase transition from cubic to orthorhombic that was observed in this experiment coincides with the calculated transition (27 GPa) from the magnetic to the nonmagnetic regime and the sudden change in the oxygen positions, calculated by Kaewmaraya *et al.* [22]. In their work they attributed these changes to the collapse of the magnetic moments of Co^{+2}. Unfortunately, the subtle difference in the positions reported by the calculations is within the error bar of the values obtained during the refinements.

Sequential refinements allowed to obtain an experimental curve of the unit cell volume as a function of pressure. The Vinet model [Eq. (1)] was used to fit the pressure dependence of the volume for the cubic and orthorhombic phases (Fig. 4) [33]. The value of K_0' was fixed to 4 due to the strong correlation between the parameters. The obtained values are presented in Table I and the corresponding fittings are displayed in Fig. 4. The K_0 values obtained from the fitting of the cubic phase are in good agreement with the previously reported [21] for the system. The values for the orthorhombic phase cannot be compared since this is the first time this phase

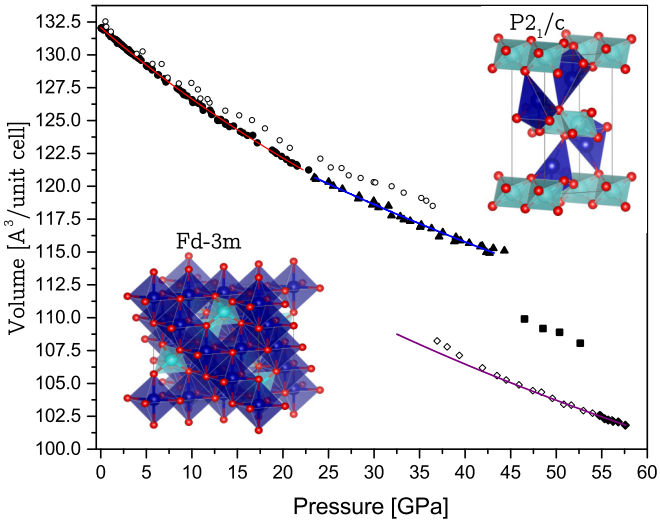

FIG. 4. Volume per formula unit of the unit cell as a function of pressure for the cubic, orthorhombic, and $P2_1/c$ monoclinic phases of Co_3O_4. The compression values are shown in full symbols and the decompression values in hollow symbols. The corresponding Vinet equation fittings are presented in full lines. The crystal structures of the cubic and the $P2_1/c$ monoclinic phases are also shown. In this drawing, the light and dark blue polyhedrons show the position of the Co^{+2} and Co^{+3} ions with their respective coordination number. Red spheres correspond to O atoms.

is reported:

$$P = 3K_0\left(\frac{V}{V_0}\right)^{-2/3}\left[1-\left(\frac{V}{V_0}\right)^{1/3}\right] \times \exp\left\{\frac{3}{2}(K_0'-1)\left[1-\left(\frac{V}{V_0}\right)^{1/3}\right]\right\}. \quad (1)$$

In Fig. 4 it is possible to observe that there is no unit cell volume difference between the cubic and the orthorhombic phase, which is in agreement with the second order character of the transition. Besides, it is possible to notice that at pressures close to 45 GPa the volume uncertainty increases, presenting a much higher variance between successive points. This behavior can be attributed to the presence of the second highest pressure phase, which has some overlapping peaks that make the refinement much more complex in this region. The presence of this second phase also made difficult to estimate the FWHM of the peaks belonging to the cubic phase due to the overlapping of the reflections.

At pressures above 52 GPa, the peaks of the orthorhombic phase disappear completely and the peaks corresponding to the third phase become more prominent. In Fig. 2(c), a LeBail refinement using a $C2/m$ crystal structure is presented for the data acquired at 52 GPa. The calculated lattice parameters are presented in the Table II. This new phase has not been previously reported in the literature, and as can be noticed from the figure, it was not possible to obtain a clean diffractogram of it due to its coexistence with the low pressure one.

The results show that the intermediate high pressure phase $C2/m$ coexists with the orthorhombic phase from 43 to 52 GPa, and with the following high pressure phase from 52 to 55 GPa. At 55 GPa, the $C2/m$ phase disappears completely. Several attempts to find the atoms location using the superflip algorithm were performed without success. The mentioned overlapping of the peaks made impossible the refinement of the atomic positions from the acquired data due to the discrepancy generated in reflections intensities. This also induced more dispersion in the volume per formula unit determination, as it can be seen in Fig. 4 within the 45–55 GPa region.

TABLE II. Refined lattice parameters of the two high pressure crystal structures.

Phase	a (Å)	b (Å)	c (Å)	β
$C2/m$ @ 52 GPa	5.44(5)	8.13(5)	5.76(3)	117.9(3)
$P2_1/c$ @ 57 GPa	2.59(3)	8.34(5)	4.91(4)	105.2(2)

The last phase was fitted with a $P2_1/c$ crystal structure and the results are shown in Fig. 2(d). The lattice parameters are presented in Table II. The atomic positions were determined using the Rietveld refinement method. The obtained results, presented in Table III, show good agreement with the values previously calculated using DFT methods [22], except for the case of O^{-2} atoms.

$P2_1/c$ structure was predicted [22] to be stable at much lower pressures (35 GPa). A similar phase was also reported [20] by Hirai and Mao, although with very different lattice parameters. As predicted by Kaewmaraya *et al.* [22], the obtained $P2_1/c$ structure is layered along the [001] direction and the Co^{+2} coordination number increases from 4, in the cubic and orthorhombic phases, to 6, in the monoclinic $P2_1/c$ one, as shown in the inset of Fig. 4. It remains to be determined the coordination number of Co^{+2} in the $C2/m$ phase, in order to establish if the octahedral $Co(II)O_6$ clusters are formed during this last phase transition or if they appear in the orthorhombic to $C2/m$ phase transition.

Upon decompression, the system remained in the $P2_1/c$ phase down to 35 GPa. At this pressure the transition towards the initial cubic phase started. This transition finished at 30 GPa, pressure at which only the peaks belonging to the cubic phase were evidenced. The evolution of the diffraction data collected during decompression is presented in the right part of Fig. 1. Results of the refinements of the two phases upon decompression are presented in Figs. 2(e) and 2(f). As it can be observed, the refinements present good agreement, indicating that these two phases are the only ones present during the decompression process. Volume per formula unit variation with pressure for both phases, spinel and monoclinic $P2_1/c$, was calculated using the data obtained from the refinements. The results are presented in Fig. 4 as hollow

TABLE III. Refined atomic positions for the $P2_1/c$ phase at 57 GPa.

Atom	x	y	z
Co^{+2}	0.00	0.00	0.00
Co^{+3}	0.77(2)	0.32(3)	0.98(4)
O^{-2}	0.44(2)	0.45(2)	0.14(3)
O^{-2}	0.74(3)	0.10(5)	0.16(4)

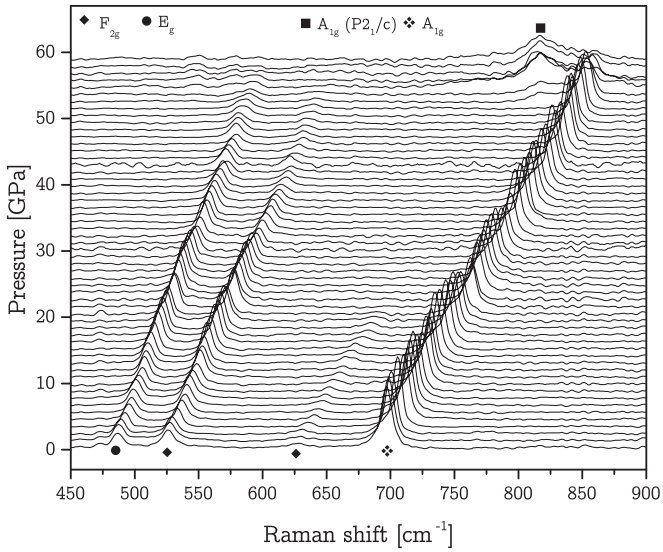

FIG. 5. Raman sequence showing the evolution of the Raman spectra during compression. The symbols mark the different modes assigned to the peaks observed.

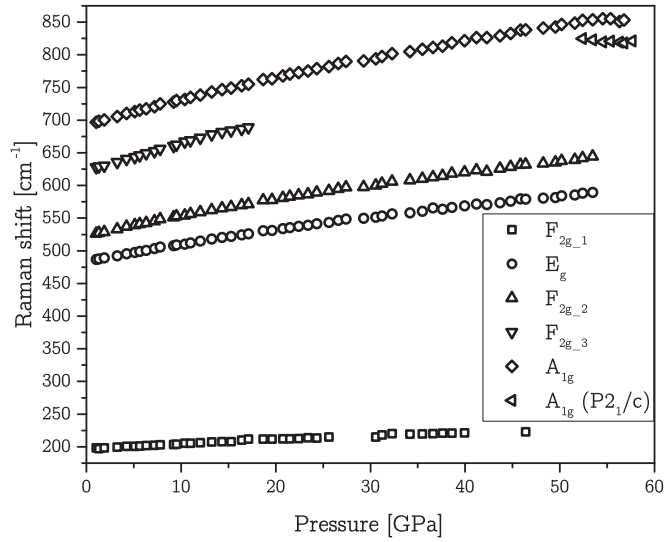

FIG. 6. Evolution of the Raman modes with pressure.

symbols. As it can be seen from the figure, the volume change with pressure of the monoclinic phase follows the same curve during compression and decompression. However, the volume of the cubic phase observed during decompression is slightly higher than the volumes obtained when compressing to the same pressure. A possible explanation for this is a reduction of the particle size that occurred during the successive phase transitions, which lead to the formation of much smaller particles with a higher surface. The presence of more atoms on the surface of the material can lead to a subtle expansion of the lattice. This explanation is supported by the results obtained from refinements and the broadening of all the peaks observed after the decompression [see Fig. 2(f)]. The absence of the $C2/m$ structure during decompression combined with the fact that it does not appear without the presence of a second phase during the compression may be an indication that this phase could be a metastable one. More experiments are planned to clarify and deeply study the stability of this phase.

In order to gain a better understanding of the high pressure behavior of Co_3O_4, Raman spectrometry measurements were performed. For that, a DAC was loaded with the sample and compressed up to 60 GPa. The normal spinel Co_3O_4 is known to have five characteristic Raman active modes at atmospheric pressure: at 196, 523, 621 (F_{2g}), 482 (E_g), and 693 cm^{-1} (A_{1g}) [14,34]. According to Bai *et al.* [21] the first and third F_{2g} modes cannot be observed at pressures higher than 15 and 20 GPa, respectively. To the best knowledge of the authors, there is no report of Raman active modes in the high pressure phase $P2_1/c$.

Figure 5 shows the evolution of the Raman spectra during compression. As it can be observed, the A_{1g} Raman mode remains active up to 52 GPa and then slowly starts to fade. This mode is usually associated with the symmetric stretching of the $Co^{+2} - O$ bond in the tetrahedral sites [35,36], so its disappearance during the transition from $C2/m$ to $P2_1/c$ phases indicates that in the $C2/m$ phase the coordination number of the Co^{+2} ions is still 4.

Similarly to the results presented by Bai *et al.* [21], the third F_{2g} mode disappeared at 20 GPa. However, in these measurements it was possible to observe the first F_{2g} up to around 40 GPa. Furthermore, it is possible to notice that the other two Raman modes observed at room pressure (E_g and the second F_{2g}) become progressively less intense at 45 GPa and disappear after reaching 53 GPa, indicating that their presence in the spectra is due to the remaining $Fddd$ phase. Given that the F_{2g} and E_g modes are forbidden in $C2/m$ [37], these results support the selection of $C2/m$ as the space group for the third phase.

The A_{1g} mode is present after the $Fddd$ to $C2/m$ phase transition with the same shift as before, indicating the tetrahedral character of the coordination between the Co^{+2} in the $C2/m$ phase. The position of this mode indicates that the $Co^{+2} - O$ bond length in this phase is similar to the observed in the $Fddd$ and Fd-$3m$ phases. When the system starts the transition to the high pressure phase $P2_1/c$, the A_{1g} previously measured starts to lose intensity and a new mode arises at lower frequency (813 vs 858 cm^{-1} for the A_{1g} mode at 55 GPa). At 57 GPa, where the phase transition is completed, the new mode is the only one present in the spectra, as it can be observed from Fig. 5. Due to the value of the shift observed for this peak, it is possible to speculate that it is associated with the symmetric stretching of the $Co^{+2} - O$ bond, like in all the previous phases, with the difference that in this case the Co^{+2} ions are in the center of the octahedron instead of tetrahedrons. If this is the case, it would be possible to assign the peaks to the A_g mode of the $P2_1/c$ phase. The shift towards lower values indicates that in this new structure the bond length in the octahedral configuration is larger than in the tetrahedral configuration presented in the previous structures. These results are in agreement with the calculations reported by Kaewmaraya *et al.* [22], in which a larger $Co^{+2} - O$ bond for the $P2_1/c$ phase at high pressures is reported and it is related to the increment in the coordination number.

The evolution of the Raman modes of Co_3O_4 with pressure is presented in Fig. 6. It is possible to notice that the A_{1g} mode splits at pressures above 52 GPa, and the initial A_{1g} mode

disappears after completing the transition at 56 GPa, leaving only the new A_g mode observed at lower frequencies.

IV. CONCLUSIONS

The behavior of Co_3O_4 at pressures up to 60 GPa was studied using structural and vibrational characterization methods. An equation of state in agreement with some of the previously reported values was obtained and two new phase transitions were observed in addition to the already predicted/reported one.

Using high pressure synchrotron powder x-ray diffraction, a first phase transition was observed at 25 GPa and turned out to be a distortion of the ambient pressure Fd-$3m$ cubic phase into an orthorhombic phase, where the atomic positions were roughly maintained. A second transition from the orthorhombic phase to the intermediate high pressure $C2/m$ phase was observed between 45 and 52 GPa. Finally, at 52 GPa the system transformed to a $P2_1/c$ phase which has also been theoretically predicted. At 57 GPa only this last phase could be observed indicating the end of the transition. Raman spectroscopy measurements on Co_3O_4 performed at high pressures supported the results obtained by x-ray diffraction.

In this work, it was possible to obtain the lattice parameters and atomic positions of the $P2_1/c$ phase, most of which presented good agreement with the calculated ones [22]. During decompression the system showed a considerable hysteresis, retaining the last high pressure phase, $P2_1/c$, down to a pressure more than 20 GPa lower than the transition pressure observed during compression. Due to this hysteresis, the two intermediate pressure phases were not present during the system decompression.

Raman studies allowed us to determine that the Co^{+2} ions were forming $Co(II)O_4$ tetrahedrons in the three lower pressure structures, and that their coordination changes to 6 to form $Co(II)O_6$ octahedrons in the $P2_1/c$ phase with larger Co^{+2}–O bond. These results experimentally confirm the calculations performed previously by Kaewmaraya *et al.* [22].

ACKNOWLEDGMENT

The authors would like to thank European Synchrotron Radiation Facility (ESRF) for in-house beamtime allocation and financial support.

[1] D. Bergman, J. Alicea, E. Gull, S. Trebst, and L. Balents, Order-by-disorder and spiral spin-liquid in frustrated diamond-lattice antiferromagnets, Nat. Phys. **3**, 487 (2007).

[2] P. Poizot, S. Laruelle, S. Grugeon, L. Dupont, and J.-M. Tarascon, Nano-sized transition-metal oxides as negative-electrode materials for lithium-ion batteries, Nature (London) **407**, 496 (2000).

[3] O. Zaharko, A. Cervellino, V. Tsurkan, N. B. Christensen, and A. Loidl, Evolution of magnetic states in frustrated diamond lattice antiferromagnetic $Co(Al_{1-x}Co_x)_2O_4$ spinels, Phys. Rev. B **81**, 064416 (2010).

[4] S. K. Pandey, S. Khalid, N. P. Lalla, and A. V. Pimpale, Local distortion in $LaCoO_3$ and $PrCoO_3$: Extended x-ray absorption fine structure, x-ray diffraction and x-ray absorption near edge structure studies, J. Phys.: Condens. Matter **18**, 10617 (2006).

[5] J. Mu, L. Zhang, G. Zhao, and Y. Wang, The crystal plane effect on the peroxidase-like catalytic properties of Co_3O_4 nanomaterials, Phys. Chem. Chem. Phys. **16**, 15709 (2014).

[6] E. Barrera, T. Viveros, A. Montoya, and M. Ruiz, Titaniumtin oxide protective films on a black cobalt photothermal absorber, Solar Energy Mater. Solar Cells **57**, 127 (1999).

[7] X. Xie, Y. Li, Z.-Q. Liu, M. Haruta, and W. Shen, Low-temperature oxidation of CO catalysed by Co_3O_4 nanorods, Nature (London) **458**, 746 (2009).

[8] M. Ando, T. Kobayashi, S. Iijima, and M. Haruta, Optical recognition of CO and H_2 by use of gas-sensitive $Au - Co_3O_4$ composite films, J. Mater. Chem. **7**, 1779 (1997).

[9] E. L. Salabas, A. Rumplecker, F. Kleitz, F. Radu, and F. Schuth, Exchange anisotropy in nanocasted Co_3O_4 nanowires, Nano Lett. **6**, 2977 (2006).

[10] J. Park, X. Shen, and G. Wang, Solvothermal synthesis and gas-sensing performance of Co_3O_4 hollow nanospheres, Sensors Actuators B **136**, 494 (2009).

[11] N. Zhang, J. Shi, F. Niu, J. Wang, and L. Guo, A cocatalyst-free Eosin Y-sensitized p-type of Co_3O_4 quantum dot for highly efficient and stable visible-light-driven water reduction and hydrogen production, Phys. Chem. Chem. Phys. **17**, 21397 (2015).

[12] C. N. P. da Fonseca, M.-A. De Paoli, and A. Gorenstein, The electrochromic effect in cobalt oxide thin films, Adv. Mater. **3**, 553 (1991).

[13] L. Yan, X. Zhang, T. Ren, H. Zhang, X. Wang, and J. Suo, Superior performance of nano-Au supported over Co_3O_4 catalyst in direct N_2O decomposition, Chem. Commun. **8**, 860 (2002).

[14] Y. Lou, J. Liang, Y. Peng, and J. Chen, Ultra-small Co_3O_4 nanoparticles—Reduced graphene oxide nanocomposite as superior anodes for lithium-ion batteries, Phys. Chem. Chem. Phys. **17**, 8885 (2015).

[15] D. Liu, X. Wang, X. Wang, W. Tian, Y. Bando, and D. Golberg, Co_3O_4 nanocages with highly exposed {110} facets for high-performance lithium storage, Sci. Rep. **3**, 2543 (2013).

[16] Z. Chen, C. X. Kronawitter, and B. E. Koel, Facet-dependent activity and stability of Co_3O_4 nanocrystals towards the oxygen evolution reaction, Phys. Chem. Chem. Phys. **17**, 29387 (2015).

[17] D.-E. Jiang and S. Dai, The role of low-coordinate oxygen on Co_3O_4 (110) in catalytic-CO oxidation, Phys. Chem. Chem. Phys. **13**, 978 (2010).

[18] Y. Jo, J.-G. Park, H. C. Kim, W. Ratcliff, and S.-W. Cheong, Pressure-dependent magnetic properties of geometrically frustrated $ZnCr_2O_4$, Phys. Rev. B **72**, 184421 (2005).

[19] H. Ueda and Y. Ueda, Pressure-enhanced direct exchange coupling observed in chromium spinels, Phys. Rev. B **77**, 224411 (2008).

[20] S. Hirai and W. Mao, Novel pressure-induced phase transitions in Co_3O_4, Appl. Phys. Lett. **102**, 041912 (2013).

[21] L. Bai, M. Pravica, Y. Zhao, C. Park, Y. Meng, S. Sinogeikin, and G. Shen, Charge transfer in spinel Co_3O_4 at high pressures, J. Phys.: Condens. Matter **24**, 435401 (2012).

[22] T. Kaewmaraya, W. Luo, X. Yang, P. Panigrahi, and R. Ahuja, A new, layered monoclinic phase of Co_3O_4 at high pressure, Phys. Chem. Chem. Phys. **17**, 19957 (2015).

[23] S. Klotz, J.-C. Chervin, P. Munsch, and G. L. Marchand, Hydrostatic limits of 11 pressure transmitting media, J. Phys. D: Appl. Phys. **42**, 075413 (2009).

[24] N. Tateiwa and Y. Haga, Evaluations of pressure-transmitting media for cryogenic experiments with diamond anvil cell, Rev. Sci. Instrum. **80**, 123901 (2009).

[25] H. K. Mao, J. Xu, and P. M. Bell, Calibration of the ruby pressure gauge to 800 kbar under quasi-hydrostatic conditions, J. Geophys. Res.: Solid Earth **91**, 4673 (1986).

[26] A. P. Hammersley, S. O. Svensson, M. Hanfland, A. N. Fitch, and D. Hausermann, Two-dimensional detector software: From real detector to idealised image or two-theta scan, High Press. Res. **14**, 235 (1996).

[27] B. H. Toby and R. B. V. Dreele, What's new in GSAS-II, Powder Diffr. **29**, S2 (2014).

[28] J. Rodriguez-Carvajal, Recent advances in magnetic structure determination by neutron powder diffraction, Physica B **192**, 55 (1993).

[29] L. Palatinus and G. Chapuis, SUPERFLIP a computer program for the solution of crystal structures by charge flipping in arbitrary dimensions, J. Appl. Crystallogr. **40**, 786 (2007).

[30] V. Petricek, M. Dusek, and L. Palatinus, Crystallographic Computing System JANA2006: General features, Z. Kristallogr. Cryst. Mater. **229**, 345 (2014).

[31] W. Roth, The magnetic structure of Co_3O_4, J. Phys. Chem. Solids **25**, 1 (1964).

[32] J. P. Picard, G. Baud, J. P. Besse, and R. Chevalier, Croissance cristalline et etude structurale de Co_3O_4, J. Less-Common Met. **75**, 99 (1980).

[33] P. Vinet, J. R. Smith, J. Ferrante, and J. H. Rose, Temperature effects on the universal equation of state of solids, Phys. Rev. B **35**, 1945 (1987).

[34] L. M. Alrehaily, J. M. Joseph, and J. C. Wren, Radiation-induced formation of Co_3O_4 nanoparticles from Co^{2+}(aq): Probing the kinetics using radical scavengers, Phys. Chem. Chem. Phys. **17**, 24138 (2015).

[35] V. G. Hadjiev, M. N. Iliev, and I. V. Vergilov, The Raman spectra of Co_3O_4, J. Phys. C: Solid State Phys. **21**, L199 (1988).

[36] H. Shirai, Y. Morioka, and I. Nakagawa, Infrared and Raman spectra and lattice vibrations of some oxide spinels, J. Phys. Soc. Jpn. **51**, 592 (1982).

[37] D. L. Rousseau, R. P. Bauman, and S. P. S. Porto, Normal mode determination in crystals, J. Raman Spectrosc. **10**, 253 (1981).